



# **An Investigation of Drag on the Haack Series Nose Cones through Subsonic and Supersonic Mach Regimes**

By

**Chad O'Brien**

**An Honors Thesis submitted in partial fulfillment of the requirements for the Honors Diploma to**

**The Honors College  
of  
The University of Alabama in Huntsville**

**29 April 2014**

## **Abstract**

In fulfillment with the requirements of the Honors College, Senior Design MAE 493, and the Charger Rocket Works - NASA Student Launch team, this thesis provides a drag analysis comparison between the LV Haack and a LD Haack nose cones using computational fluid dynamics (CFD) methods. It is desirable to determine sectional drag coefficients through the subsonic and supersonic Mach regimes for scaling and predictive purposes. The primary goal was to observe the effects that slenderness ratio and cross sectional area have on nose cone drag. It utilized the aide of CFD-ACE+, a multiphysics modeling and simulation software suite to provide numerical results for the full Navier Stokes equations including compressible aerodynamics and energy equations. The target Mach regimes were primarily the subsonic and supersonic transition regions which start and end at Mach 0.8 and Mach 1.2 respectively. Due to predicted flight speeds of the Senior Design high powered rocket, a complete analysis covered Mach 0.3 to Mach 1.7 in 0.2 increments with refinement in sonic barrier region. This studied observed that drag coefficient is primarily a function of slenderness ratio. As the slenderness ratio increases, the pressure and viscous components of drag behave differently between the subsonic and supersonic regions. In the subsonic, an increase of slenderness shows growth of the viscous drag considerably while the drag due to pressure seems relatively unaffected. However, in the supersonic region the viscous term decrease as well as the pressure term with respect to an increase in slenderness.

**Honors Thesis Advisor**  
Dr. David Lineberry

Advisor:

Date:

Department Chair:

Date:

Honors College Director:

Date:

# An Investigation of Drag on the Haack Series Nose Cones through Subsonic and Supersonic Mach Regimes

Chad O'Brien  
Honors College  
University of Alabama in Huntsville  
Huntsville, Alabama 35899

Advisor: David Lineberry, Ph.D.

29 April 2014

## Abstract

In fulfillment with the requirements of the Honors College, Senior Design MAE 493, and the Charger Rocket Works - NASA Student Launch team, this thesis provides a drag analysis comparison between the LV Haack and a LD Haack nose cones using computational fluid dynamics (CFD) methods. It is desirable to determine sectional drag coefficients through the subsonic and supersonic Mach regimes for scaling and predictive purposes. The primary goal was to observe the effects that slenderness ratio and cross sectional area have on nose cone drag. It utilized the aid of CFD-ACE+, a multiphysics modeling and simulation software suite to provide numerical results for the full Navier Stokes equations including compressible aerodynamics and energy equations. The target Mach regimes were primarily the subsonic and supersonic transition regions which start and end at Mach 0.8 and Mach 1.2 respectively. Due to predicted flight speeds of the Senior Design high powered rocket, a complete analysis covered Mach 0.3 to Mach 1.7 in 0.2 increments with refinement in sonic barrier region. This studied observed that drag coefficient is primarily a function of slenderness ratio. As the slenderness ratio increases, the pressure and viscous components of drag behave differently between the subsonic and supersonic regions. In the subsonic, an increase of slenderness shows growth of the viscous drag considerably while the drag due to pressure seems relatively unaffected. However, in the supersonic region the viscous term decrease as well as the pressure term with respect to an increase in slenderness.

## Nomenclature

$C_d$	Coefficient of Drag, non-dimensional
$f$	Slenderness Ratio – Length vs Diameter, non-dimensional
$x$	Relation Distance from an Origin for nose cone profile geometry, in
$R_{base}$	Base Nose Cone Radius, in
$R(x)$	Radius of the nose cone as a function of $x$ , in
$v$	Velocity, ft/s
$q$	Dynamic Pressure, psi
$S$	Reference Area, in <sup>2</sup>
$\rho$	Density, lbm/ft <sup>3</sup>
$F$	Force, lbf
$L$	Length, in
$R^*$	Air's Ideal Gas Constant, ft <sup>2</sup> /(s <sup>2</sup> -R)
$Re$	Reynolds Number, non-dimensional
$\mu$	Dynamic Viscosity, lbm/(ft-s)
$M$	Mach Number, non-dimensional
$\gamma$	Air's Ratio of Specific Heat, non-dimensional

## I. Introduction

Wolfgang Haack, an aerodynamicist from Germany theorized that there was an optimal geometry for a given aerodynamic profile. Through linearized flow theory, he established a series of nosecone that is the solution to the minimized drag for a given body's length and diameter or volume. For a similar length and diameter or volume body, Eq. (2) mathematically describes the revolved profile.

$$\theta(x) = \arccos\left(1 - \frac{2x}{L}\right) \quad (1)$$

$$R(x, C) = \frac{R_{base}}{\sqrt{\pi}} \sqrt{\theta(x) - \frac{\sin(2\theta(x))}{2} + C\sin(\theta(x))^3} \quad (2)$$

In Eq. (2), the variable  $C$  will be optimized for the nose cone profile that identifies the minimized drag for a given length and volume ( $C=1/3$ ) known as the LV-HAACK (aka Von Karman Ogive) and minimized drag for a given length and diameter ( $C=0$ ) LD-HAACK. A set of radius, combined with a set of slenderness ratios will be used to create a collection of nose cones that will be used in the Computation Fluid Dynamics solver CFD-ACE+ to determine the numerical drag solution to these well-defined shapes.

The CFD Solver will output a force acting on different surfaces from which we will be able to calculate the total drag coefficient using Eq. (3) through Eq. (7) along with the pressure and viscous drag coefficients in Eq. (8).

$$F = qSCd \quad (3)$$

$$q = \frac{1}{2}\rho v^2 \quad (4)$$

$$S = \pi R^2 \quad (5)$$

$$Cd = \frac{F}{qS} \quad (6)$$

$$Cd = \frac{2F}{\rho v^2 S} \quad (7)$$

$$Cd_{total} = Cd_{viscous} + Cd_{pressure} \quad (8)$$

$$Cd_{total} = \frac{2}{\rho v^2 S} (F_{viscous} + F_{pressure}) \quad (9)$$

Often times it is useful to determine what type of flow is involved in a simulation by comparing Reynolds Number. Reynolds Number is the ratio of a fluid's inertial force to its viscous forces. The higher the Reynolds number is the more turbulent the fluid and typically it also reduces the effective viscosity. For flow over a body, the Reynolds Number with respect to length is the defined by Eq. (10).

$$Re_L = \frac{\rho V_{ref} L}{\mu} \quad (10)$$

This number will affect the mesh creation in that the more turbulent the region, the more nodes and thus high mesh density for regions of higher turbulence. The regions will occur near walls and no slip conditions; where the fluid is being altered by the represented nose cone body.

Figure 1 are results from a NACA report on nose cones with slenderness 3. The top plot is the results from an LV Haack nose cone while the bottom plot is the results of an LD Haack nose cone. These plots detail the drag at the upper range of this thesis project but will still be useful in verifying the upper limit solution reliability.

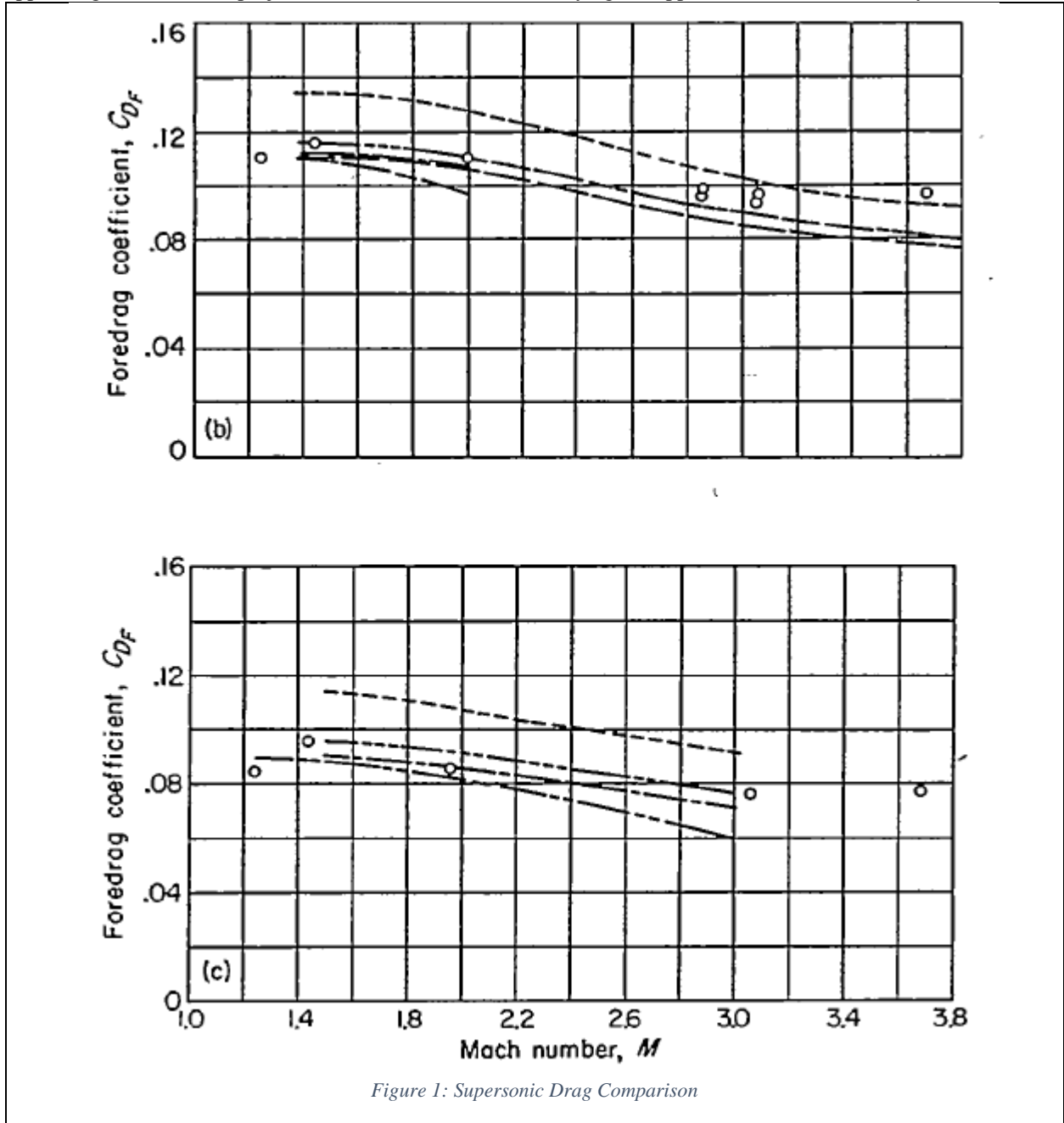


Figure 1: Supersonic Drag Comparison

## II. Model

### A. Nose Cone Geometry Combinations

In effort to assist the research into model rocketry, common radii were used that would be near matches to the set of general nose cones for high powered and low powered rockets. Then some simplification to area was applied to allow for easy non-dimensional analysis of the output. The “recipe” for the collection of nose cones prescribed by the combination of the following variables is defined below, where  $R$  is the radius,  $f$  is the slenderness ratio,  $L$  is the length,  $D$  is the diameter,  $C$  defines the two separate nose cones, and  $S$  is the resulting reference cross sectional base area. Overall, there were 18 nosecones with unique dimensions. Radii normalized to the square root of pi was used in effort to simplify dynamic pressure calculations and area ratios by providing integer areas.

$$R_{base} = \frac{1}{\sqrt{\pi}} \left\{ \frac{1}{2}, 1, 2 \right\} \text{ in} \quad (11)$$

$$f = \left( \frac{L}{D} \right) = \{3, 4, 5\} \quad (12)$$

$$L = 2 \prod (R_{base} \times f) \quad (13)$$

$$\prod (R_{base} \times f) = \left\{ \prod (r, f_i) \mid r \in R_{base} \wedge f_i \in f \right\} \quad (14)$$

$$C = \left\{ 0, \frac{1}{3} \right\} \quad (15)$$

Figure 3 shows a detail of the 3D nose cone that was modeled in 2D. Figure 2 details the LD and LV Haack nose cone’s differences in a graphical representation of the two profiles defined by Eq. (1) and Eq. (2).

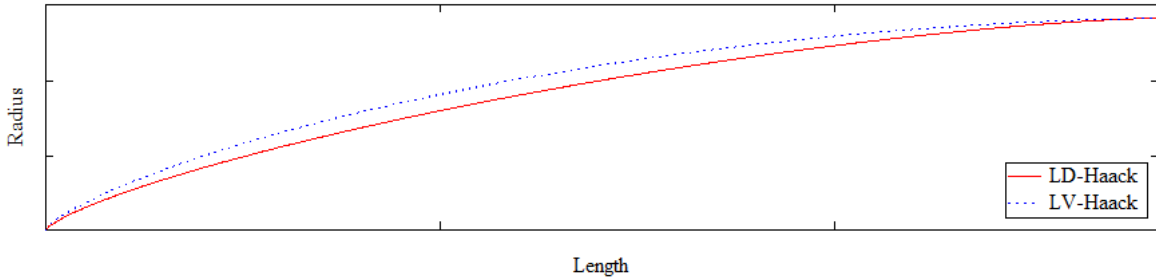


Figure 2: General Profiles

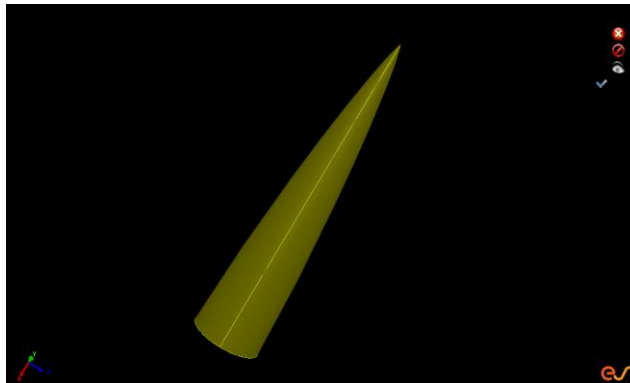


Figure 3: Nosecone Solid

## B. Geometry Creation

CFD-ACE+ software suite contains its own proprietary geometry creator called CFD-GEOM®. It provides the end user with an integrated development environment which can be used to create and visualize the regions of mesh, nodes, gridlines, and geometry as well as dynamically name boundaries and volumes which provides the user the ability to identify nodes and groups of nodes. Using the naming scheme, users can quickly identify specific boundaries and apply the necessary conditions to simulate their model. Figure 4 defines these boundaries in the general model.

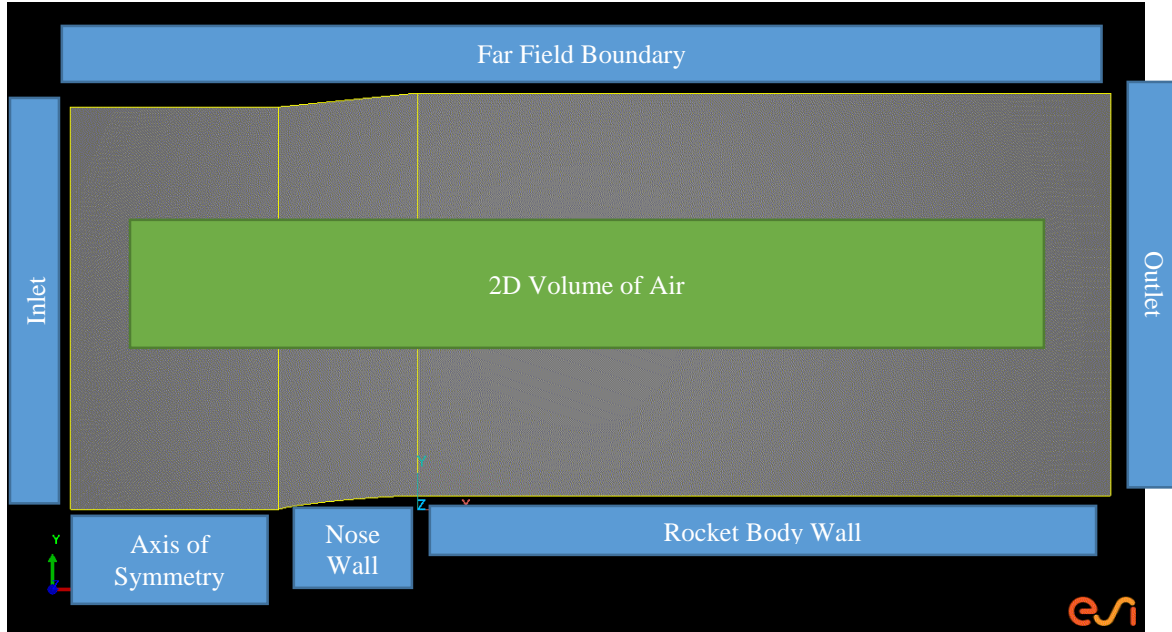


Figure 4: 2D Model

In order to perform this study efficiently, python scripting was used to customize the general model with the sets of dimensions listed in Section A. This automatically created the shown geometry and labeled the boundaries and volumes appropriately so a common nomenclature is observed through all 18 models. CFD-ACE utilizes its own python based application programming interface (API) which assisted in the creation of the geometry shown. The scripts can be found in the appendix. Section D will discuss the meaning and settings of the names in Figure 4.

## C. Mesh Creation

CFD-ACE+ uses finite difference schemes to solve the multiphysics equations involved in the solution. The user must first generate a grid of points called nodes, these nodes will exist in regions to define the location of the boundary conditions and interior volumes of the fluid. The solution is directly related to the resolution of the nodes near critical features. Since this study involved solving the equations for supersonic flow, turbulence, and heat transfer, special considerations were made to node creation near the walls of the nose and rocket body. In order to accurately capture the Mach shock at the nose and viscous effects along the walls, fine mesh must be created in these regions. Figure 5

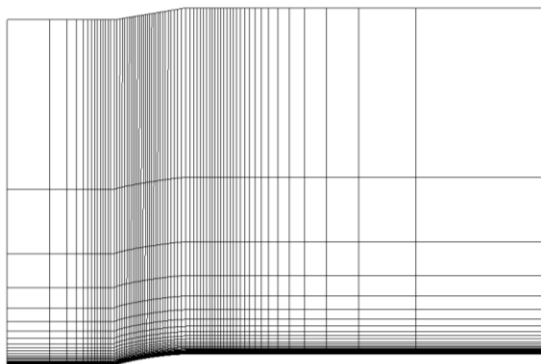


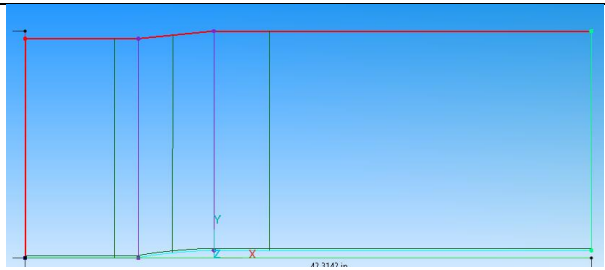
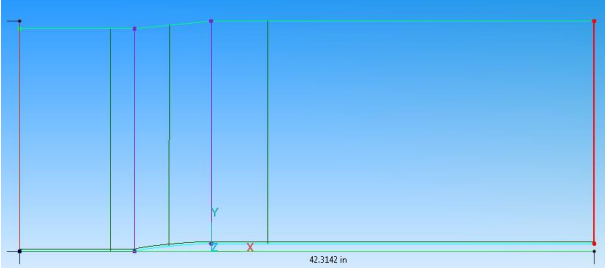
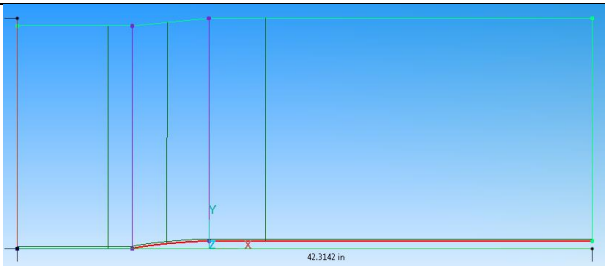
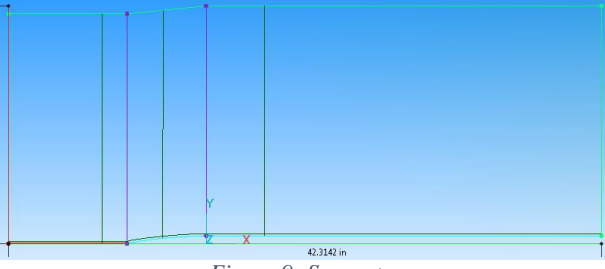
Figure 5: Volume Mesh

shows the trends of the mesh along the X direction of the geometry. There is a much higher mesh density near the nose cone that will capture the thermal changes due to compressible aerodynamics and to provide a resolution that will capture the Mach shock. It will be weak due to the size of the nose cone and the amount of air that will be undergoing this shock. The thick black line near the walls is an area of high refinement. Depending on the turbulence model selected, this mesh density will change to the selected model's unique parameter called Y-Plus ("y + "). This will be discussed in section D. Boundary and Volume conditions.

### D. Boundary and Volume Conditions

CFD-ACE-GUI was used to apply certain conditions to the model boundaries and volumes. In an attempt to reduce the complexity of the problem, several conditions were assumed such as dissipation rates, kinetic energy at boundaries, pressure, velocities, and thermal heating. Figure 4 through Figure 9 details 6 main boundaries and 1 volume which Table 1 breaks down the specifics of each which are highlighted in red.

Table 1: Boundary Condition Settings

Boundary Name	Conditions	Reference
Farfield	$\vec{V} = V_{ref} \hat{i} + 0\hat{j} + 0\hat{k};$ $P = P_{ref} = 100kPa$ $T_{backflow} = 300K$ $Dissipation_{backflow} = 0 \frac{J}{kg}$ $Kinetic Energy_{backflow} = 0 \frac{J}{kg}$	 <p>Figure 6: Farfield</p>
Exit (Extrapolated)	$T_{backflow} = 300K$ $P = P_{ref} = 100kPa$ $Dissipation_{backflow} = 0 \frac{J}{kg}$ $Kinetic Energy_{backflow} = 0 \frac{J}{kg}$	 <p>Figure 7: Extrapolated Exit</p>
Wall (No-Slip)	$\vec{V} = 0\hat{i} + 0\hat{j} + 0\hat{k}$ <i>Adiabatic</i> <i>Roughness = 20μm</i>	 <p>Figure 8: Wall Conditions</p>
Symmetry	<i>Conditions on Modeled Side are the same as revolved.</i> <i>Axi-Symmetric Reference.</i>	 <p>Figure 9: Symmetry</p>

### 1. Farfield Condition

This model assumes that the boundaries are distanced far enough away that the events and fluid physics during shock dissipate before it gets to the boundaries. This means that the local flows at the fluid boundaries, with the exception of the outlet, are the same. The inlet velocity,  $V_{ref}$ , is determined by which Mach value is run.

The Mach values were chose based on common low powered to high powered speeds that are expected for hobby rockets and ranges from Mach 0.3 to Mach 1.7 with a step of Mach 0.2. In an effort to characterize the effects of crossing the sonic barrier, the step size was reduced to Mach 0.02 between Mach 0.9 and Mach 1.1. The input is in SI units and Eq. (16) will convert the input Mach value to velocity.

$$V = M(\sqrt{\gamma R^* T}) \quad (16)$$

### 2. Exit - Extrapolated

The outlet was given an extrapolated condition because it extends from the wall of the body to the outer boundary. There will be a fluid velocity gradient along this boundary due to viscous effects which the solver will determine as part of the solution.

### 3. Wall conditions

Keeping true to the focus of hobby rocket modeling, it is assumed that the aerothermal heating occurs for such a short time that the material and wall does not have time to be heated. Therefore, the wall conditions are set to adiabatic. The roughness effects the viscous terms through the turbulence model K-epsilon ( $K - \epsilon$ ). It was mentioned previously that the grid was defined based on the Y-Plus value of a turbulence model and in this case the Y-Plus is 30. The value is an output off the solver run, therefore the grid generation was an iterative process of creating a mesh, running the case, and then adjusting the meshed based on the Y-Plus output.

### 4. Symmetry

The axi-symmetric model uses an axis of symmetry to make the assumption the model is mirror and rotationally symmetric. This is what allows for the simplification of a full 3D simulation into 2D. When an axi-symmetric model is run, the solver artificially revolves the model one radian to create a 3D model for density, energy, mass, and other 3D calculations. The results are therefore in per unit radian and the true solution to the theoretical 3D fully rotated nose can be determined by multiplying the results by  $2\pi$ .

## E. Model Resolution and Convergence Criteria

The solver uses the full Navier Stokes with viscous flow and energy equations to iteratively determine the solution to the flow field. The numerical methods applied could result in a time and resource intensive process therefore limits are applied. A convergence residual was set at  $10^{-8}$  and the total iterations were set at 7500. The limit that was achieved first ended the solver run. This convergence rate to the specified residual is dependent on the mesh and precautions were made to ensure the accurate solutions were reached. The high mesh density in the region of high compression assists.

The boundary conditions are set to simplify the case even further. Through iterative solver runs, the outer boundary distance was increased until the Mach shocks no longer intersected with the boundary. The Farfield condition assumes that the boundaries are far enough away such that the conditions represent the flow infinitely far away and uninfluenced by the solid body.

The rocket body was incorporated and extends to the exit boundary to eliminate the based drag that occurs. This thesis was designed to determine the drag characteristics of the nose cone of hobby rockets. Therefore, the body was extruded behind the nose cone to eliminate base drag.

The total simulation set of 306 unique cases were automated using python scripts and the built-in API functions for the CFD-ACE+ Suite. Each case generated approximately 2800 cells for the steady state simulations and took over 32 hours using an AMD® 64bit, 6-core processor and 16 GB of RAM on the Windows 7 operating system.

### III. Results

#### A. Area Comparison

The following set of figures is the results of analyzing how the slenderness ratio affects the drag for a set cross sectional area. The nomenclature for determine the nose cone and geometry is  $\langle \text{TYPE} \rangle \langle \text{Slenderness} \rangle$ . For example an LD-Haack nose cone with the slenderness ratio of 3 will have the legend name “LDF3”. Likewise, an LV-Haack nose cone will have the nomenclature “LVF3”. The naming scheme used for the figure series is that the slenderness ratio is defined by “F” and the base area is denoted in the figure titles by “A”.

##### 1. Area and Pressure Drag

Figure 10 through Figure 12 compares the drag coefficient as the base area increases. Each series in the individual figures is the drag coefficient versus mach number for the two nose cones at the slenderness ratios of 3, 4, and 5. A dynamic analysis looking for a correlation between the two nosecones of the same slenderness will show that the LV Haack on average, has approximately 14.4%, 16.8%, and 18% more drag than the LD Haack for slenderness ratios of 3, 4, and 5 respectively. The difference between the LD and LV Haack nose cones trends as maximized in the subsonic and supersonic solutions and minimized in the transonic region as shown in Figure 10. These differences are very similar when looking at the three different cross sections and may only be a result of the model’s mesh. Table 2 shows the three areas and their respective percent difference between the LV and LD Haack nose cones with each slenderness ratio. In Table 2, the observed behavior of the average difference of LV to LD is that it increases slightly between different areas and increases with slenderness ratio.

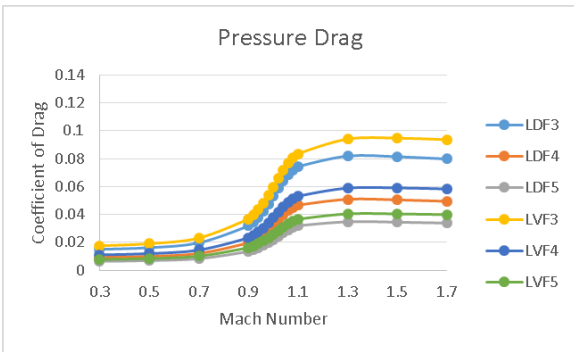


Figure 10: Pressure Drag ( $A=0.25 \text{ in}^2$ )

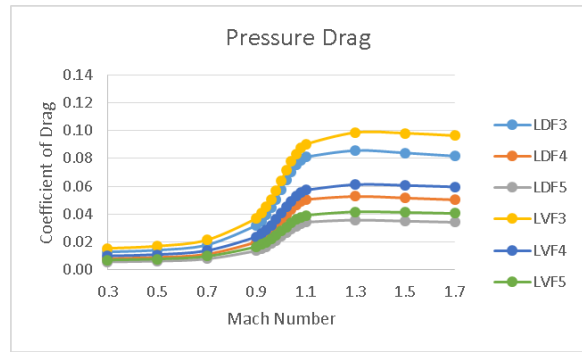


Figure 11: Pressure Drag ( $A=1.0 \text{ in}^2$ )

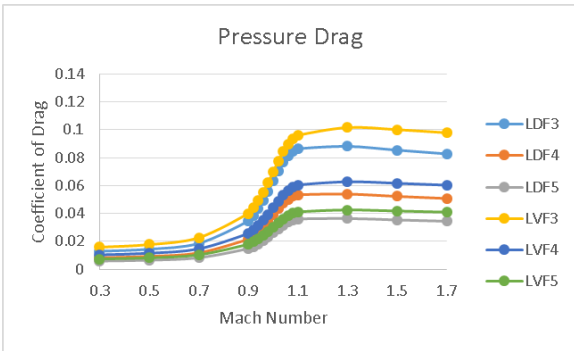


Figure 12: Pressure Drag ( $A=4.0 \text{ in}^2$ )

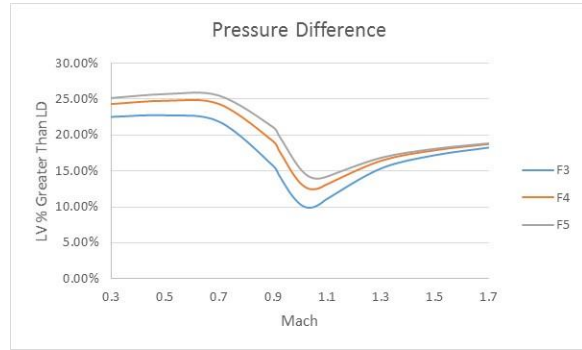


Figure 13: LV to LD Difference

Table 2: Average Relative Difference in Pressure Drag

LV % > LD	A=0.25 in <sup>2</sup>	A=1.0 in <sup>2</sup>	A=4 in <sup>2</sup>
F=3	14.62%	14.40%	14.52%
F=4	16.55%	16.69%	16.88%
F=5	17.75%	18.03%	18.25%

## 2. Area and Viscous Drag

Figure 13 through Figure 15 compare the Viscous Drag Coefficient vs Mach number through the nose cone series while each figure is a different cross sectional area. It is observable that the viscous drag is dependent on the base area. However, it is not directly due to base area, but more due to surface area which is a function of the radius and length. The viscous drag drops as the base area increases. A study would need to be looked at to see how the localized flow transforms based on geometry. It would seem reasonable that the viscous drag is lower with the increase in area due to the gradient of the nose cone. As the radius increases, the gradient for a given slenderness ratio increases which could induce localized turbulence, thus reducing the viscous drag during certain portions of the nose cone. Further analysis needs to be performed to confirm this assumption. Also, the viscous drag decreases with an increase of Mach number which correlates to an increase in turbulence. As the turbulence increases, eddies form near the boundary which have varying viscosity which, as expected, reduces the effective viscosity and therefore reduces the total viscous force.

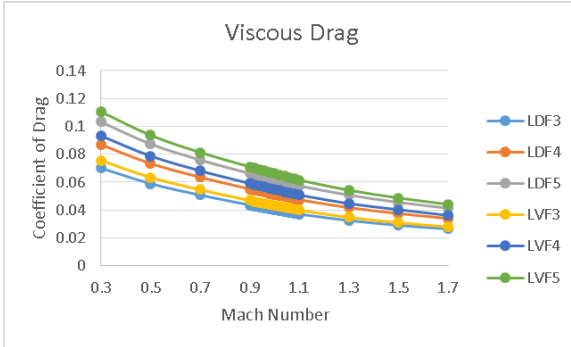


Figure 14: Viscous Drag ( $A=0.25 \text{ in}^2$ .)

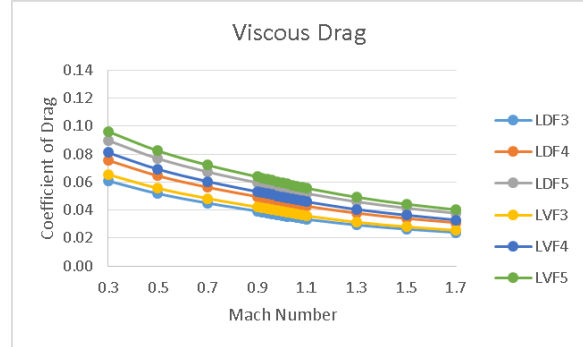


Figure 15: Viscous Drag ( $A=1.0 \text{ in}^2$ )

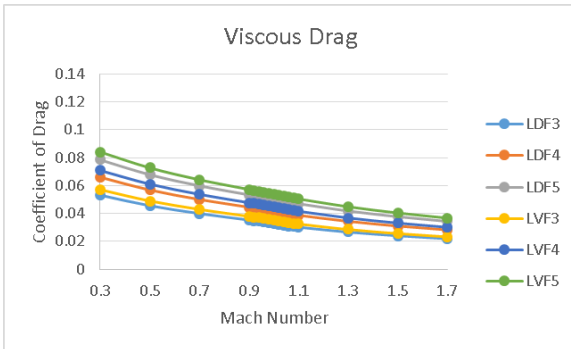


Figure 16: Viscous Drag ( $A=0.25 \text{ in}^2$ )

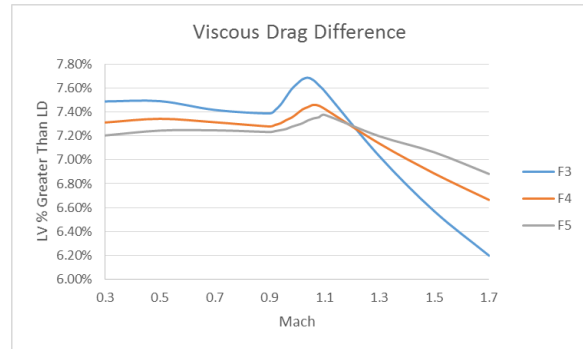


Figure 17: LV vs LD Viscous Drag Difference

Figure 16 shows the relative difference between the LV and LD Haack nose cones as a trend with the Mach number. In this case, when compared to the pressure drag relative difference, the viscous drag relative difference is greater during the transonic flow. Table 3 details the specifics of the average relative difference between the slenderness ratio and the cross sectional area. There is a small trend that as slenderness increases, the relative difference between LD and LV Haacks decrease. This may correlate to the percent difference in surface areas. For slenderness ratios 3, 4, and 5 the relative difference in surface area are 7.556%, 7.545%, and 7.540% respectively.

Table 3: Average Relative Difference in Viscous Drag

LV % > LD	A=0.25 in <sup>2</sup>	A=1.0 in <sup>2</sup>	A=4.0 in <sup>2</sup>
F=3	7.36%	7.36%	7.38%
F=4	7.24%	7.22%	7.28%
F=5	7.15%	7.17%	7.24%

## B. Slenderness Comparison

### 1. Slenderness Ratio and Pressure Drag

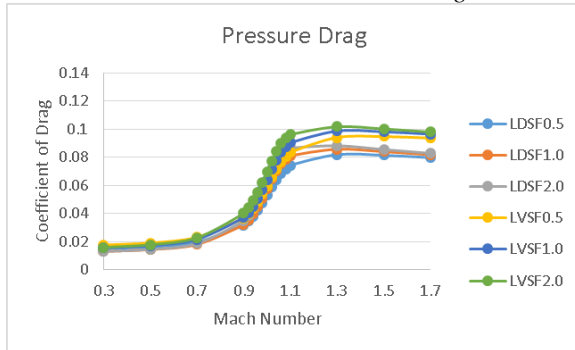


Figure 18: Pressure Drag ( $f=3$ )

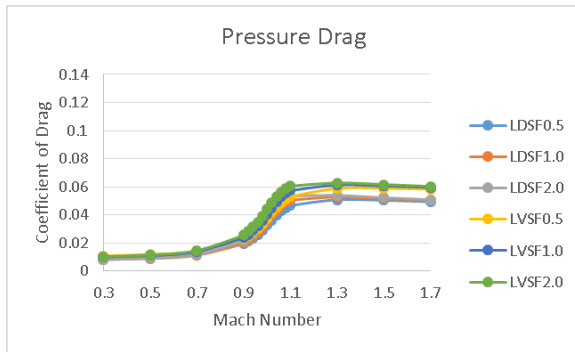


Figure 19: Pressure Drag ( $f=4$ )

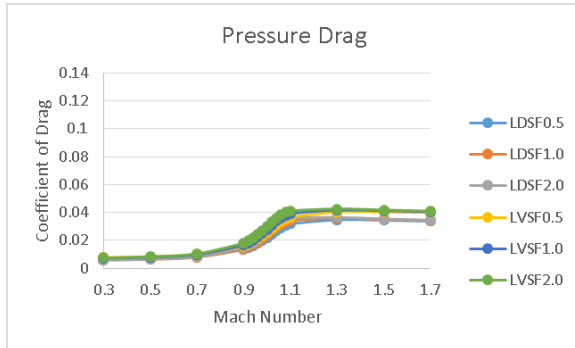


Figure 20: Pressure Drag ( $f=5$ )

The following set of figures analyzes the coefficient of drag vs. Mach number while maintaining the slenderness ratio for a given set of Areas. It is important to look at the trend of the drag coefficient as the size of the nose cone increases to predict the aerodynamics of nose cones for reasonable range sizes.

Figures 17 through Figure 19 compare how the drag changes with slenderness ratio and also looks at the individual series of areas. It is unique to see that the slenderness ratio shifts the supersonic curve differently than subsonic in that the shift displacement is not constant for all Mach values. The supersonic curve is shifted larger as the slenderness ratio goes up compared to the shift in the subsonic curve. However the results confirm the predictions that the more slender the nose, the lower the pressure drag is.

Something else that is unique about these figures is that the LD Haack and the LV Haack converge to their own solutions regardless of the cross sectional area. For subsonic cases, the drag difference between the two series of nose cones is inconsequential, however at supersonic speeds, they diverge from each other to their independent series solution. This reveals that Drag is not unique to an area but also to the nose cone profile itself. Theoretically, a drag estimate only looks at the total cross sectional area however Figure 17 through Figure 19 reveals the drag solution is unique to the profile.

Another characteristic to note is that the slenderness ratio appears to control how quickly the individual solutions converge. As the slenderness ratio goes up, the convergence rate to the two separate nose cones is faster. In Figure 18, the solution for each nose cone series has just started to converge at Mach 1.7. However, in Figure 20, the solution is nearly instantly converged just after shock. This might be attributed to the gradient of the profile. The curvature of the nose cone affects how the fluid speed increases as it flows from the tip to the base radius.

## 2. Slenderness Ratio and Viscous Drag

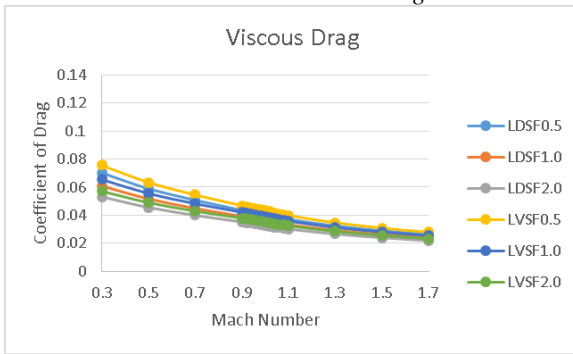


Figure 21: Viscous Drag ( $f=3$ )

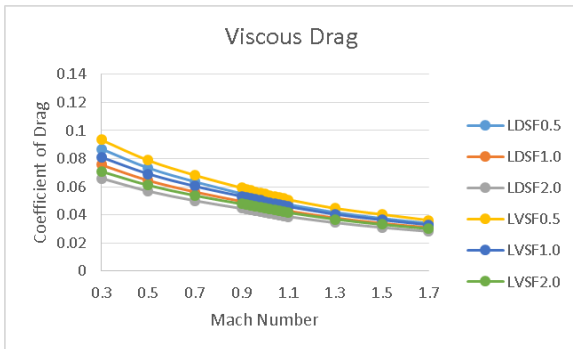


Figure 22: Viscous Drag ( $f=4$ )

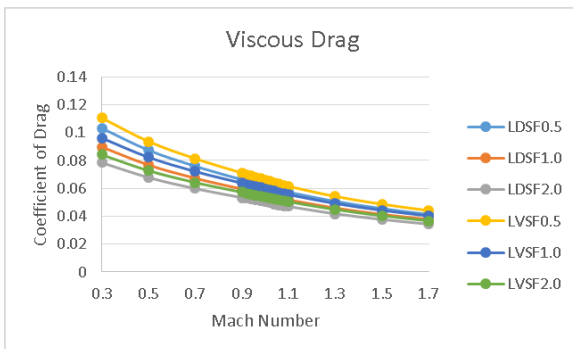


Figure 23: Viscous Drag ( $f=5$ )

Figures 20 through Figure 22 compare the viscous drag component to the mach number. Each figure is a different cross sectional area the series are the two nose cones at three different slenderness ratios. The first comparison overall that is important to recognize is within each figure, the nose cones with the largest slenderness ratio have highest viscous drag. This directly correlates to common understanding that the longer a fluid interacts with a surface, the larger the viscous forces will be. Regardless of LD or LV nosecones, the nose cones with similar slenderness ratios have similar viscous drag solutions. Within a single, slenderness value, the LV has the highest drag. In Figure 2, it is clear the LV Haack nose cone has a longer arc length. Using arc length formulas, it can be shown (see Appendix) that for any given radius, LV to LD arc length ratio decreases as slenderness increases. For the slenderness ratios of 3, 4, and 5 the LV-Haack arc length is 0.32%, 0.19%, and 0.13% longer than the LD-Haack arc length respectively. Therefore it is reasonable to make the assumption that, due to the results in Figure 12 to Figure 14, drag due to viscous effects is trends with the slenderness ratio. The larger the slenderness ratio the higher the viscous forces are. One comparison to make between Figure 21, Figure 22, and Figure 23 is that the viscous solution for subsonic is linear with area. The curves are off set slightly starting with Figure 21 and the LDF5 where the drag coefficient is approximately 0.1 and it decreases as the area increases as in Figure 13, where the area is  $1 \text{ in}^2$ , the drag coefficient is 0.09, and in Figure 23 the drag coefficient is approximately 0.08.

### C. Combined Drag

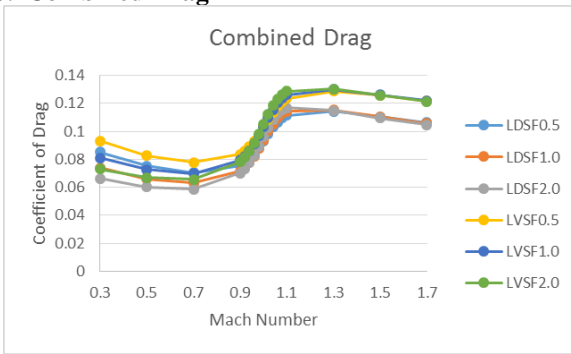


Figure 24: Combined Drag (f=3)

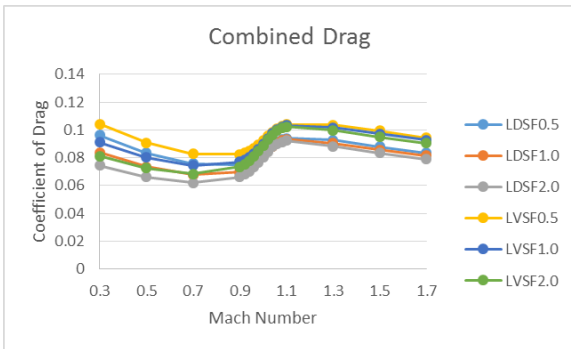


Figure 25: Combined Drag (f=4)

Figure 24 through Figure 26 contain the results which are the combination of the viscous and pressure drag solutions. Through the summation of the two forces, it is readily identifiable that the slender nose cone causes the least shift in drag during the transonic region. However, in the subsonic region the drag characteristics dictate that the drag is higher on the more slender nose cones due to viscous drag which is precisely what is confirmed. In general the, the drag on a slender nose cone is higher during the subsonic region due air's viscosity in the laminar regions. As the speed increases, the turbulence increases and viscosity decreases however the pressure drag due to Mach shocks increases.

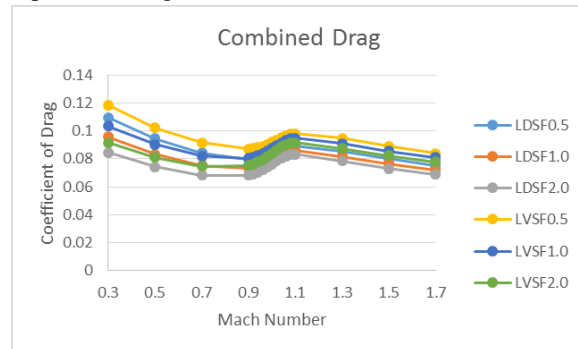


Figure 26: Combined Drag (f=5)

The supersonic total drag results correspond well with results posted in the technical report, *NACA-TR-1386*. In Figure 1, the slenderness ratio of 3 for both the LV and LD Haack are in agreement with the results posted in Figure 1. In Figure 27, the solution to supersonic flow is visualized. This particular solver uses a pressure as its integrator then solves for the other variables which sometimes has difficulty solving the Mach shock. However, the mesh was fine enough to capture these phenomena in density and Temperature.

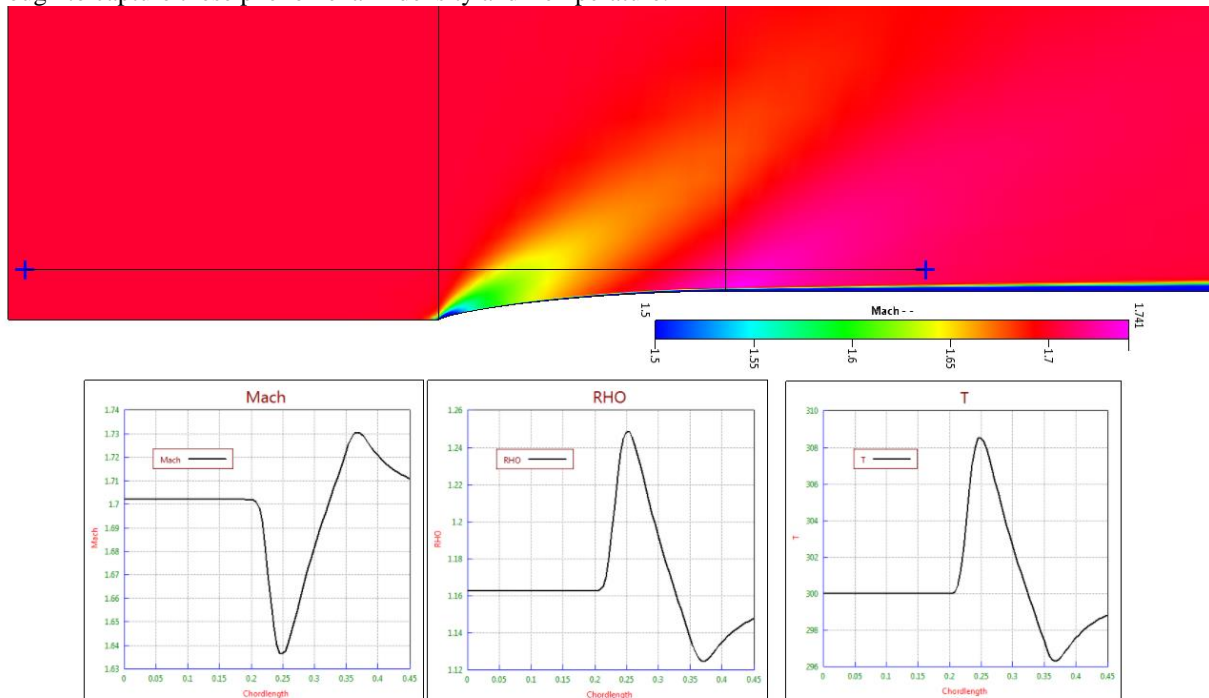


Figure 27: Mach 1.71 Inlet

#### IV. Conclusions

Through the use of computational fluid dynamics software, different generalizations were observed for the two series of nose cones in the Haack family. The LD and LV Haack nose cones were compared from Mach 0.3 through Mach 0.7 and their drag characteristics plotted. In general flow analysis, viscous drag is dependent on the surface geometry and Reynolds number. The more laminar the flow, the higher the viscous terms. As the speed of the flow increases, the Reynolds number increases until it reaches turbulent conditions. Small eddies form near surfaces in pockets and have varying viscosity values which in turn reduces the overall viscous terms which are only vis. As the slenderness ratio increase, the viscous drag increases. However, as the area increase for a single cross section, the viscous drag decreases.

While viscous drag is predominant in the subsonic region, the pressure drag increases and becomes the dominant force through the transonic and supersonic regions. The trends of pressure drag is that it increases with both slenderness and cross sectional area. However, this small difference do to area may be just an artifact of the mesh. The difference is so small that the assumption could be made that pressure drag is primarily from wave drag as the shock occurs in front of the nose cone and therefore independent of the actual dimensions since the drag term is already non dimensional relative to the cross section.

A few items need to be resolved for future cases which revolve around mesh density near the wall conditions and distance to far field conditions. If the boundary mesh is not fine enough, the viscous drag solution is less accurate as it is incapable of capturing the viscous boundary layer and other observed phenomena. Also, the size of the modeled volume will need to be verified to ensure that the shock is not influenced by the Dirchlet boundary conditions. Again, the axis-symmetric case is used to simplify symmetrically revolved models. A future study might look at mesh resolution to solution convergence and resolving the solution to curve fits using non dimensional parameters such as Mach number and Reynolds number. It would be useful to analytical correlate a Mach and Reynolds, along with geometric parameters, to drag coefficients for the nose cone.

## Appendix

### A. MATHCAD 15 Analytical Nose Analysis

## Nose Cone Calculations

**Length**  $L(f, R) := 2 \cdot R \cdot f$

**Profile**  
 $\theta(x, f, R) := \arccos\left(1 - \frac{2 \cdot x}{L(f, R)}\right)$

**Profile Equations**

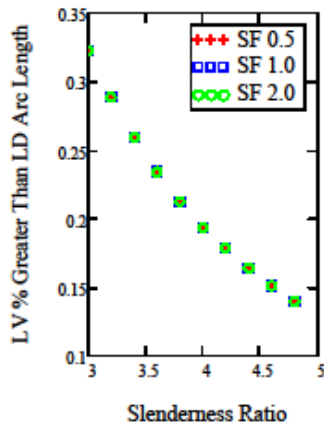
$$y(x, c, f, R) := \frac{R}{\sqrt{\pi}} \sqrt{\theta(x, f, R) - \frac{\sin(2 \cdot \theta(x, f, R))}{2} + c \cdot (\sin(\theta(x, f, R)))^3}$$

**LV Profile Arc Length**  $S_{LV}(f, R) := \int_0^{L(f, R)} \sqrt{1 + \left(\frac{d}{dx}y\left(x, \frac{1}{3}, f, R\right)\right)^2} dx$

**LD Profile Arc Length**  $S_{LD}(f, R) := \int_0^{L(f, R)} \sqrt{1 + \left(\frac{d}{dx}y(x, 0, f, R)\right)^2} dx$

**Relative Difference LV to LD**  $Rat(f, R) := \frac{|S_{LV}(f, R) - S_{LD}(f, R)|}{S_{LD}(f, R)}$

**Slenderness Ratios**  $f := 3, 3.2..5$



**Specific Slenderness Values and Radius.**

**Slenderness = 3**  $Rat\left(3, \frac{0.5}{\sqrt{\pi}}\right) = 0.3228\%$

**Slenderness = 4**  $Rat\left(4, \frac{0.5}{\sqrt{\pi}}\right) = 0.1937\%$

**Slenderness = 5**  $Rat\left(5, \frac{0.5}{\sqrt{\pi}}\right) = 0.1294\%$

Surface Area Calculations

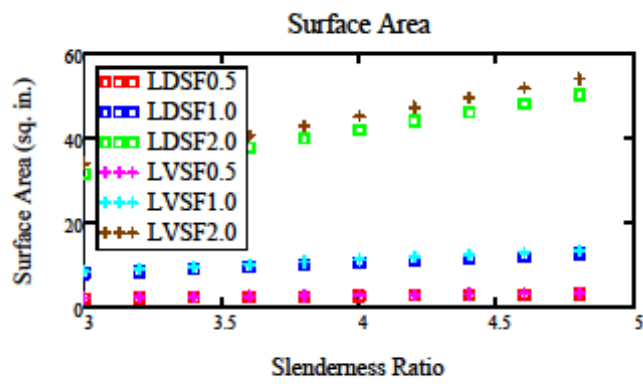
$$SA(f, R, c) := \int_0^{L(f, R)} 2\pi \cdot y(x, c, f, R) \cdot \sqrt{1 + \left(\frac{d}{dx}y(x, c, f, R)\right)^2} dx$$

LD Haack Surface Area

$$SA_{LD}(f, R) := SA(f, R, 0)$$

LV Haack Surface Area

$$SA_{LV}(f, R) := SA\left(f, R, \frac{1}{3}\right)$$



## B. Model Script

```
ModelBase.py
1  # This file was journaled by CFD-GEOM
2  import SimManager
3  import SDF
4  import GUtils
5  import GNose
6  from subprocess import call
7  from math import acos, pi, sin, pi, sqrt
8  import os
9  #GUtils.StopGeom()
10 # Note that if you plan to run this script outside CFD-GEOM,
11 # (such as in Simulation Manager or a standalone Python interpreter),
12 # please ensure that the CFD-GEOM portion of the script is wrapped
13 # by calls to GUtils.StartGeom() and GUtils.StopGeom().
14 sf=[0.5, 1.0, 2.0]
15 f = [3.0, 4.0, 5.0]
16 c = [0.0, 0.333]
17 M=[0.3, 0.5, 0.7, 0.9, 0.92, 0.94, 0.96, 0.98, 1.0, 1.02, 1.04, 1.06, 1.08, 1.1, 1.3, 1.5, 1.7]
18 a=sqrt(1.4*287*300)
19 mypath = os.getcwd()
20 for sfi in sf:
21     for ci in c:
22         for fi in f:
23             head = "sf" + str(sfi) + "_C" + str(ci) + "_E" + str(fi)
24             if not os.path.exists(head):
25                 os.makedirs(head)
26             R=1.0/sqrt(pi)*sfi
27             L=2.0*R*fi
28             GNose.nose( L, R, ci)
29             for mi in M:
30                 area = pi*(R*0.0254)**2
31                 fname = mypath + "/" + head + "/" + head + "_M" + str(mi) + ".DTF"
32                 SimManager.CopyAllAceFiles(mypath + "/MASTER_2.DTF", fname)
33                 SDF.SetBCValue(fname,"Farfield","U",mi*a)
34                 SDF.UpdateSimDoubleData(fname, 1, "OUT_FLOW_PRESSURE_COEFFICIENT_REFERENCE_VELOCITY", 0, mi*a)
35                 SDF.UpdateSimDoubleData(fname, 1, "FM_REF_AREA", 0, area)
36                 SimManager.RunSolver(fname)
37                 os.chdir(mypath)
38             # End of Mach Loop
39         # End of Slenderness Loop
40     # End of Shape Loop
41 # End of Scale Loop
```

Figure 28: Python Conditions API Script

This script is designed to handle the combination of nose cone and Mach numbers in several loops. It uses python scripting language with a built in CFD-ACE+ Suite API functions.

## C. Geometry Creator Python Script

```

1  def nose( L, R, c):
2      import GGeometry
3      import GMesh
4      import GFileIO
5      import GBCVC
6      import GUtils
7      from math import sqrt, pi, acos, sin
8      GUtils.StartGeom()
9      GUtils.SetUnits( 2 )
10     X=[0.0, 0.005, 0.01, 0.025, 0.04, 0.055, 0.07, 0.085, 0.1, 0.18, 0.26, 0.34, 0.42, 0.5, 0.6, 0.7, 0.85, 1.0]
11     nosepts=[]
12     for xi in X:
13         nx=xi*L
14         theta=acos(1.0-2.0*nx/L)
15         y=R/sqrt(pi)*sqrt(theta-sin(2.0*theta))/2.0 + c*(sin(theta))**3.0
16         nosepts.append(GGeometry.CreatePoint(nx-L,y,0.0))
17     # Created points
18     boxpts=[]
19     boxpts.append(GGeometry.CreatePoint(-2.5*L,0.0,0.0)) #0
20     boxpts.append(GGeometry.CreatePoint(5*L,30*R,0.0)) #1
21     boxpts.append(GGeometry.CreatePoint(5.0*L,R,0.0)) #2
22     boxlines=[]
23     boxlines.append(GGeometry.CreateLine(boxpts[0],nosepts[0])) #0 ____ NNNNNNNN WWWWWWWW
24     boxlines.append(GGeometry.CreateLine(boxpts[1],boxpts[2])) #1 NNNNNN WWWWWW |
25     boxlines.append(GGeometry.CreateLine(nosepts[17],boxpts[2])) #2 NNNNNN _____ |
26     noseline=GGeometry.CreateInterpolationCurve(nosepts,closed=0)
27     geom_edge1 = GMesh.CreateHyptanEdge(noseline, 30, 0, 0.07, 0.1)
28     geom_edge2 = GMesh.CreateHyptanEdge(boxlines[2], 30, 0, 0.1, 3)
29     geom_edge3 = GMesh.CreateHyptanEdge(boxlines[0], 15, 0, 1, 0.08)
30     geom_edge4 = GMesh.CreateHyptanEdge(boxlines[1], 40, 0, 4, 0.0005)
31     geom_op_faces1 = GMesh.CreateExtrudedFacesAlongEdges( geom_edge4, [geom_edge2, geom_edge3], 1, 1, 1 )
32     geom_2d_sdomain1 = GMesh.Create2DBlock( [geom_op_faces1['faces'][0], geom_op_faces1['faces'][1], geom_op_faces1['faces'][2]] )
33     GBCVC.SetBC( [geom_op_faces1['edges'][5], geom_op_faces1['edges'][2], geom_op_faces1['edges'][1], geom_op_faces1['edges'][0]], 'Farfield', 'Outlet' )
34     GBCVC.SetBC( geom_edge4, 'Exit', 'Outlet' )
35     GBCVC.SetBC( [geom_op_faces1['edges'][3], geom_op_faces1['edges'][4]], 'Interfaces', 'Symmetry' )
36     GBCVC.SetBC( geom_edge3, 'Symmetry', 'Symmetry' )
37     GBCVC.SetBC( geom_edge1, 'Nose', 'Wall' )
38     GBCVC.SetBC( geom_edge2, 'Wall', 'Wall' )
39     GBCVC.SetVC( [geom_op_faces1['faces'][0], geom_op_faces1['faces'][1], geom_op_faces1['faces'][2]], 'Air', 'Fluid' )
40     GFileIO.ExportDTF( 'MASTER_2.DTF', 2, 1, 2) # Update if possible, nosimplify,inches
41     GUtils.StopGeom()

```

Figure 29: Python Geometry API Script

This script is designed to create the necessary space shown in Figure 4. It defines the vertices and the spline interpolated nose section.

## D. Example Output from Solver

```

1 =====
2 Iteration :          370
3 =====
4 =====
5 Output for All Walls
6 =====
7 Reference Values
8 Area                Velocity                Density
9 0.161E-03           NaN                NaN
10 =====
11 Moments Reference Point
12 X                  Y                  Z
13 0.000E+00          0.000E+00          0.000E+00
14 =====
15 Pressure
16 =====
17 NAME  KEY    FX          FY          FZ          MX          MY          MZ
18 =====
19 WALL  27    0.00000E+00  0.64296E-01  0.00000E+00  0.00000E+00  0.00000E+00  0.20449E-02
20 NOSE  26    0.24626E-02  0.24438E-01  0.00000E+00  0.00000E+00  0.00000E+00  0.51891E-03
21 =====
22 Proc  1 Sum  0.24626E-02  0.88733E-01  0.00000E+00  0.00000E+00  0.00000E+00  0.25638E-02
23 =====
24 Viscous
25 =====
26 NAME  KEY    FX          FY          FZ          MX          MY          MZ
27 =====
28 WALL  27    0.55599E-01  0.00000E+00  0.00000E+00  0.00000E+00  0.00000E+00  -0.39838E-03
29 NOSE  26    0.11537E-01  0.15466E-02  0.00000E+00  0.00000E+00  0.00000E+00  -0.96826E-04
30 =====
31 Proc  1 Sum  0.67136E-01  0.15466E-02  0.00000E+00  0.00000E+00  0.00000E+00  -0.49521E-03
32 =====
33 Pressure and Viscous Sum
34 =====
35 NAME  KEY    FX          FY          FZ          MX          MY          MZ
36 =====
37 WALL  27    0.55599E-01  0.64296E-01  0.00000E+00  0.00000E+00  0.00000E+00  0.16465E-02
38 NOSE  26    0.13999E-01  0.25984E-01  0.00000E+00  0.00000E+00  0.00000E+00  0.42209E-03
39 =====
40 Proc  1 Sum  0.69599E-01  0.90280E-01  0.00000E+00  0.00000E+00  0.00000E+00  0.20686E-02
41 =====

```

Figure 30: Example Wall Reaction Forces

Figure 28 is a snap shot of a “FMSUM” file which records the Force and Moment. The shell script in Figure 29 is programmed to grab the Viscous and Pressure Terms from these files. This study generated 306 unique cases and a script was needed to efficiently compile the data.

## E. Shell Script for Data Collection

```

ModelBase.py  GNose.py  sf0.5_C0.0_F3.0_M0.3.FMSUM  parseFMSUM.sh
1  #!/bin/sh
2  for d in $(find -type d)
3  do
4      grep -m 1 "NOSE" ${d}/*.FMSUM | awk '{print $4}' > ${d}/pressure.txt
5      grep -m 2 "NOSE" ${d}/*.FMSUM | awk 'NR%2 == 0' | awk '{ print $4 }' > ${d}/viscous.txt
6  done

```

Figure 31: Shell FMSUM Parse Code

Figure 29 is a simple code to search through all the directories created from the script in Figure 26. It will loop through each directory, looking specifically for the FMSUM files. It will read through each FMSUM file pulling only the requested data from the text files and adding them to reduced files name “Pressure.txt” and “viscous.txt”. These files were imported into excel and further manipulated to provide the plots provided in this report.

**F. Axial Force from Pressure – Raw Data**

*Table 4: Axial Force from Dynamic Pressure*

Mach/File	LD-HAACK									LV-HAACK								
	SF_0.5			SF_1.0			SF_2.0			SF_0.5			SF_1.0			SF_2.0		
	F3	F4	F5	F3	F4	F5	F3	F4	F5	F3	F4	F5	F3	F4	F5	F3	F4	F5
0.3	0.0025	0.0015	0.0011	0.0085	0.0055	0.0039	0.0340	0.0219	0.0156	0.0029	0.0018	0.0013	0.0102	0.0066	0.0048	0.0417	0.0273	0.0196
0.5	0.0074	0.0045	0.0031	0.0261	0.0166	0.0117	0.1056	0.0677	0.0479	0.0087	0.0054	0.0038	0.0313	0.0203	0.0144	0.1296	0.0845	0.0603
0.7	0.0176	0.0108	0.0074	0.0643	0.0406	0.0285	0.2667	0.1696	0.1192	0.0207	0.0130	0.0091	0.0771	0.0498	0.0353	0.3250	0.2108	0.1495
0.9	0.0470	0.0290	0.0199	0.1894	0.1184	0.0817	0.8197	0.5114	0.3515	0.0543	0.0343	0.0239	0.2191	0.1408	0.0987	0.9485	0.6093	0.4257
0.92	0.0534	0.0330	0.0226	0.2189	0.1366	0.0939	0.9529	0.5926	0.4055	0.0615	0.0389	0.0271	0.2513	0.1612	0.1126	1.0912	0.6991	0.4866
0.94	0.0613	0.0379	0.0259	0.2556	0.1592	0.1089	1.1185	0.6934	0.4719	0.0703	0.0445	0.0308	0.2910	0.1863	0.1296	1.2671	0.8093	0.5607
0.96	0.0710	0.0439	0.0299	0.3011	0.1871	0.1273	1.3230	0.8177	0.5532	0.0810	0.0512	0.0354	0.3399	0.2169	0.1502	1.4832	0.9439	0.6504
0.98	0.0828	0.0511	0.0347	0.3563	0.2209	0.1496	1.5685	0.9672	0.6506	0.0939	0.0593	0.0408	0.3991	0.2539	0.1748	1.7429	1.1052	0.7570
1	0.0965	0.0596	0.0403	0.4203	0.2603	0.1754	1.8484	1.1382	0.7620	0.1089	0.0687	0.0471	0.4677	0.2968	0.2033	2.0403	1.2901	0.8788
1.02	0.1114	0.0690	0.0466	0.4890	0.3030	0.2037	2.1431	1.3198	0.8814	0.1253	0.0790	0.0540	0.5419	0.3436	0.2345	2.3567	1.4879	1.0098
1.04	0.1264	0.0786	0.0531	0.5565	0.3456	0.2324	2.4255	1.4958	0.9994	0.1417	0.0896	0.0613	0.6156	0.3905	0.2663	2.6654	1.6822	1.1404
1.06	0.1403	0.0876	0.0594	0.6175	0.3845	0.2594	2.6735	1.6519	1.1069	0.1572	0.0997	0.0683	0.6836	0.4342	0.2965	2.9441	1.8584	1.2612
1.08	0.1528	0.0958	0.0652	0.6702	0.4182	0.2831	2.8814	1.7825	1.1990	0.1715	0.1090	0.0749	0.7441	0.4728	0.3235	3.1860	2.0101	1.3670
1.1	0.1641	0.1030	0.0704	0.7160	0.4468	0.3035	3.0571	1.8909	1.2760	0.1845	0.1174	0.0808	0.7980	0.5064	0.3471	3.3971	2.1397	1.4576
1.3	0.2526	0.1570	0.1073	1.0578	0.6512	0.4420	4.3526	2.6626	1.7996	0.2903	0.1818	0.1247	1.2174	0.7565	0.5154	5.0206	3.0999	2.1026
1.5	0.3343	0.2072	0.1415	1.3800	0.8486	0.5761	5.6179	3.4388	2.3277	0.3891	0.2425	0.1660	1.6127	0.9976	0.6787	6.5840	4.0539	2.7489
1.7	0.4208	0.2609	0.1784	1.7255	1.0627	0.7230	6.9900	4.2901	2.9115	0.4940	0.3075	0.2105	2.0350	1.2587	0.8571	8.2663	5.0945	3.4604

In Table 4, the listed values are directly collected from the FMSUMparse.sh shell routine showing in Figure 29. These were manipulated into non-dimensional calculations and plotted in the results section of this report. The values listed are in units of Newtons (N), the “F” is the slenderness ratio, and the “SF” is the radial scaling factor.

**G. Axial Force from Viscous Effects – Raw Data**

*Table 5: Viscous Force*

Mach/File	LD-HAACK									LV-HAACK								
	SF_0.5			SF_1.0			SF_2.0			SF_0.5			SF_1.0			SF_2.0		
	F3	F4	F5	F3	F4	F5	F3	F4	F5	F3	F4	F5	F3	F4	F5	F3	F4	F5
0.3	0.0115	0.0143	0.0170	0.0400	0.0497	0.0590	0.1398	0.1737	0.2064	0.0124	0.0153	0.0182	0.0430	0.0533	0.0632	0.1503	0.1864	0.2213
0.5	0.0269	0.0335	0.0399	0.0945	0.1178	0.1403	0.3332	0.4156	0.4954	0.0290	0.0360	0.0428	0.1015	0.1263	0.1504	0.3582	0.4462	0.5313
0.7	0.0455	0.0569	0.0680	0.1611	0.2017	0.2410	0.5729	0.7175	0.8575	0.0488	0.0610	0.0728	0.1730	0.2163	0.2583	0.6154	0.7700	0.9196
0.9	0.0645	0.0815	0.0980	0.2324	0.2935	0.3523	0.8361	1.0537	1.2637	0.0694	0.0875	0.1051	0.2496	0.3146	0.3775	0.8979	1.1304	1.3551
0.92	0.0664	0.0839	0.1010	0.2391	0.3024	0.3635	0.8618	1.0875	1.3052	0.0714	0.0901	0.1083	0.2570	0.3244	0.3895	0.9257	1.1668	1.3997
0.94	0.0682	0.0863	0.1039	0.2457	0.3112	0.3745	0.8868	1.1210	1.3465	0.0734	0.0926	0.1114	0.2643	0.3339	0.4014	0.9529	1.2029	1.4441
0.96	0.0700	0.0887	0.1067	0.2522	0.3198	0.3852	0.9108	1.1538	1.3875	0.0754	0.0952	0.1145	0.2713	0.3433	0.4131	0.9793	1.2384	1.4882
0.98	0.0718	0.0910	0.1096	0.2585	0.3283	0.3958	0.9338	1.1859	1.4279	0.0773	0.0977	0.1176	0.2781	0.3525	0.4246	1.0047	1.2731	1.5318
1	0.0735	0.0933	0.1125	0.2645	0.3365	0.4062	0.9560	1.2171	1.4677	0.0791	0.1002	0.1207	0.2847	0.3614	0.4359	1.0290	1.3070	1.5747
1.02	0.0752	0.0956	0.1153	0.2705	0.3447	0.4165	0.9777	1.2476	1.5069	0.0809	0.1026	0.1237	0.2911	0.3702	0.4470	1.0527	1.3402	1.6170
1.04	0.0768	0.0979	0.1182	0.2764	0.3528	0.4268	0.9993	1.2779	1.5457	0.0827	0.1050	0.1267	0.2974	0.3789	0.4580	1.0761	1.3730	1.6590
1.06	0.0785	0.1001	0.1210	0.2824	0.3611	0.4371	1.0214	1.3083	1.5844	0.0845	0.1074	0.1297	0.3037	0.3876	0.4690	1.0997	1.4059	1.7008
1.08	0.0802	0.1024	0.1238	0.2885	0.3694	0.4475	1.0443	1.3392	1.6232	0.0862	0.1098	0.1328	0.3102	0.3965	0.4801	1.1239	1.4390	1.7426
1.1	0.0820	0.1047	0.1267	0.2948	0.3779	0.4580	1.0678	1.3706	1.6621	0.0881	0.1123	0.1358	0.3168	0.4055	0.4913	1.1487	1.4724	1.7847
1.3	0.1003	0.1290	0.1566	0.3624	0.4670	0.5675	1.3186	1.6998	2.0660	0.1072	0.1379	0.1675	0.3873	0.5000	0.6078	1.4113	1.8211	2.2147
1.5	0.1194	0.1541	0.1872	0.4336	0.5593	0.6804	1.5813	2.0404	2.4818	0.1272	0.1657	0.2001	0.4615	0.5986	0.7273	1.6852	2.1809	2.6571
1.7	0.1394	0.1796	0.2185	0.5065	0.6556	0.7985	1.8504	2.3872	2.9033	0.1476	0.1911	0.2329	0.5393	0.6960	0.8505	1.9651	2.5463	3.1031

In Table 5, the listed values are directly collected from the FMSUMparse.sh shell routine showing in Figure 29. These were manipulated into non-dimensional calculations and plotted in the results section of this report. The values listed are in units of Newton (N), the “F” is the slenderness ratio, and the “SF” is the radial scaling factor.

## **Acknowledgments**

Chad O'Brien would like to thank ESI-CFD for their support in donating a license for using their software. Also, the expertise and advice given by Sami Bayyuk from ESI-CFD regarding the model creation and solutions. His insight was very useful in identifying areas for grid optimization and cell formation near boundary conditions. C. O'Brien would also like to thank Dr. David Lineberry from the University of Alabama in Huntsville for his expertise and guidance in modeling compressible flow. Dr. Lineberry served as the primary adviser for this project.

## **References**

### *Technical Report*

Perkins, E., and Jorgensen, L. , and Sommer, S., "Investigation of the Drag of Various Axially Symmetric Nose Shapes of Fineness Ratio 3 for Mach Numbers from 1.24 to 7.4", NACA-TR-1386, Jan. 1958.

### *Books*

Moore, Frank G., *Approximate Methods for Weapon Aerodynamics*, American Institute of Aeronautics and Astronautics, Inc., Danvers, MA, 2000

Anderson, John D., *Fundamentals of Aerodynamics, 5<sup>th</sup> Ed.*, McGraw-Hill, New York, NY, 2007.